Turkish Journal of Electrical Engineering & Computer Sciences

http://journals.tubitak.gov.tr/elektrik/

Research Article

Turk J Elec Eng & Comp Sci
(2013) 21: 2048 – 2061

doi:10.3906/elk-1202-114

Detection of microcalcification clusters in digitized X-ray mammograms using unsharp masking and image statistics

Pelin KUŞ,[1,*] **İrfan KARAGÖZ**[2]

[1]Department of Electronics Engineering, Turkish Military Academy, Dikmen, Ankara, Turkey
[2]Department of Electrical and Electronics Engineering, Faculty of Engineering,
Gazi University, Maltepe, Ankara, Turkey

Received: 28.02.2012 • **Accepted:** 14.06.2012 • **Published Online:** 24.10.2013 • **Printed:** 18.11.2013

Abstract: A fully automated method for detecting microcalcification (MC) clusters in regions of interest (ROIs) extracted from digitized X-ray mammograms is proposed. In the first stage, an unsharp masking is used to perform the contrast enhancement of the MCs. In the second stage, the ROIs are decomposed into a 2-level contourlet representation and the reconstruction is obtained by eliminating the low-frequency subband in the second level. In the third stage, statistical textural features are extracted from the ROIs and they are classified using support vector machines. To test the performance of the method, 57 ROIs selected from the Mammographic Image Analysis Society's MiniMammogram database are used. The true positive and false positive rates are used to evaluate the performance of the classification, and the results are compared with those from other studies presented in the literature. The results show that the classification method of unsharp masking and low-band eliminated image statistics is convenient for MC cluster detection. In particular, a true positive rate of about 94% is achieved at the rate of 0.06 false positives per image.

Key words: Image analysis, microcalcification detection, mammography, Mammographic Image Analysis Society database, classification, support vector machines

1. Introduction

Breast cancer is the most common type of cancer among women [1]. Some important signs of breast cancer that radiologists are seeking to find are microcalcifications (MCs), masses, and structural disorders. MCs are observed in mammograms as white spots varying in size and shape. Important characteristics are their size, shape/morphology, amount, and distribution. Their sizes vary from 0.1 mm to 1 mm [2]. MC detection is very difficult in mammographies with overlapping breast tissues or high breast tissue density. Moreover, low-contrast MCs can be perceived as noise while comparing them with the nonhomogeneous background. MCs are observed in mammograms individually or in clusters. Clustered MCs are more likely to be malignant. A cluster is defined as a group consisting of 3 or more MCs in a 1-cm^2 area. As proposed in this study, many computer-aided detection systems have been developed for MCs.

In [3], Yu and Guan first segmented out potential MC pixels in the mammograms using both multiresolution and gray-level statistical features. Next, using a set of 31 features (mean, standard deviation, edge, foreground and background ratio, area, compactness, elongation, moments, contrast, entropies, correlation, variance, etc.), they grouped the detected individual MCs into clusters depending on their relative positions.

*Correspondence: pkus@kho.edu.tr

Jing et al. [4] investigated the spatial distribution of MC clusters in mammograms. They modeled MCs and background noise by gamma and Gaussian distribution, respectively. They also modeled the interaction of neighbor MCs with each other by a marked point process. The MCs were then segmented via a maximum a posteriori estimation. Halkiotis et al. [5] detected clustered MCs using mathematical morphology and artificial neural networks. Yu and Huang [6] used combined model-based and statistical textural features to investigate the performance of clustered MC recognition in mammograms. Nishikawa et al. [7] used morphological erosion to reduce the false positives (FPs) after taking the difference image of 2 filter outputs, the first for enhancing the MCs and the second for suppressing them. McLoughlin et al. [8] proposed a noise equalization scheme. In this method, the quantum noise was illustrated using the square root of the gray levels. Qian et al. [9] applied a cluster analysis-based region grouping approach for MC detection. The study of Linguraru et al. [10] included image filtering based on anisotropic diffusion and curvilinear structure removal using local energy and phase congruency. Gürcan et al. [11] used higher-order statistics (skewness, kurtosis). That study made the assumption that the areas without MCs resemble a Gaussian distribution and the areas with MCs resemble non-Gaussian. In [12], a mammogram was decomposed into subbands using a nonlinear filter bank. In the subbands, the regions with high positive skewness and kurtosis values were marked as regions of interest (ROIs). Afterwards, the MC locations were detected using an outlier labeling method. Caputo et al. used a generalized Gaussian kernel energy function in a Markov random field (MRF) model for MC detection [13]. Casaseca-de-la-Higuera et al. [14] compared different approaches based on Gaussian mixture models. MRF models define the spatial gray level intensity distribution of an image. However, estimating the proper distribution is difficult in these probabilistic approaches. Sankar and Thomas [15] used fractal analysis to model breast texture using the local self-similarity. Huang et al. [16] proposed a new fast fractal image coding method for MC detection in ROIs. Oliver et al. [17] built a dictionary using extracted local features using Sobel, Laplace, and Gaussian filters to obtain a local description of the morphology of MCs. This dictionary was used to test data.

Strickland and Hahn [18] used a lossless undecimated biorthogonal wavelet transform. Mini et al. [19] implemented wavelet transform, utilizing the pseudo-periodicity property of the image sequences. Nakayama et al. [20] developed a filter bank based on the Hessian matrix to classify nodular and linear structures. Regentova et al. [21] used wavelet transforms and hidden Markov trees. Rizzi et al. [22] reduced background noise by thresholding mammograms through a biorthogonal wavelet filter according to the images' statistical parameters: mean and standard deviation. In order to detect MCs, they decomposed the reconstructed image with an orthogonal wavelet and processed each decomposition level using a hard threshold technique. The disadvantage of this method is that the parameter used in the algorithm depends on the database. Some of the studies used machine learning in order to extract dependencies within the data.

Jiang et al. [23] and Peng et al. [24] proposed methods based on evolutionary genetic algorithms. Jiang et al. performed MC detection and classification with the genetic algorithm, using 3 domains: pixel domain, feature domain consisting of the local mean and variances, and cluster domain. Peng et al. used the knowledge discovery mechanism incorporated with the genetic algorithm to improve the performance of the method. After transforming the data from the pixel domain to the feature domain using the mean and standard deviation, they selected 5 group centers to define the genes. These genes constituted the chromosomes that were used to search for the bright spots in the mammogram. In [25–28], neural networks were investigated. However, the main disadvantage of the neural networks is trapping in the local minima.

Support vector machines were recently stated to reach high accuracy in MC detection in the literature [29,30]. El Naqa et al. [29] improved the detection rate by applying a successive enhancement learning procedure.

Wei et al. [30] used a Bayesian learning approach (a relevance vector machine) to predict the MCs. Many studies showed that machine learning methods are powerful classifiers. However, in these methods, overfitting the data is also possible in cases where independent datasets or statistical resampling methods are not used. Compared with the other methods, machine learning methods showed the best results.

Andreadis et al. [31] applied various feature extraction methods on ROIs with MCs to compare their performance in terms of classification accuracy and discriminating power. They put forth that the combination of all of the features improves the classification accuracy, with a performance better than that of individual groups. Mohanalin et al. [32] used a type II fuzzy index for automatic MC detection. The thresholding was performed with Tsallis entropy using a type II fuzzy index. Their results showed that the proposed Tsallis entropy approach was better than the 2-dimensional nonfuzzy approach and the conventional Shannon entropy partition approach. Dheeba and Tamil [33] applied support vector machines using Laws' texture energy measures to determine for each pixel whether it is an MC or not.

The purpose of this study is to achieve a fully automated detection of the MC clusters in digitized mammograms. To this end, with the help of support vector machines, a classification of the texture features of the high-frequency components extracted from mammogram images with enhanced contrast is made. From the preprocessed mammograms, ROIs measuring 50 $\times$ 50 pixels are selected and sharpened by the filtering operation. The filtered ROIs are decomposed into subbands, and then the feature extraction is performed from the ROIs whose approximation image is eliminated. In the final stage, the ROIs are classified using support vector machines.

The suggested MC detection method includes the main steps seen in Figure 1. Whether the ROIs contain MCs or not is discovered after they undergo the stages of image processing.

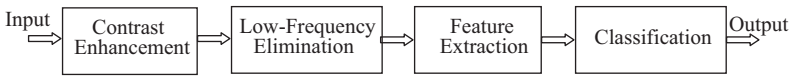

Figure 1. Block diagram of the proposed method.

2. Materials and methods

2.1. Data set

In this study, the Mammographic Image Analysis Society (MIAS) database is used [34]. Within the data, there are 2 mediolateral-oblique images belonging to each patient. The images with MCs are expressed by giving the center location of the MC cluster and the radius of the region where the MCs are distributed. The radius of the smallest MC cluster selected as the ROI is 6 pixels. The largest MC cluster distributes to the whole texture.

Each pixel in the mammogram has the dimension of 0.20 mm. Having the images in the MIAS preprocessed and setting out with the cluster definition, the ROIs with a 1-cm width and height (50 $\times$ 50 pixels) are chosen, and the method developed is applied to these ROIs. The ROIs were selected among the images of breast tissues with different densities. A total of 33 MC ROIs, consisting of 21 malignant (5 F, 8 G, and 8 D types) and 12 benign (2 F, 2 G, and 8 D types) types, and 24 ROIs of normal texture (with the 8 F, 8 G, and 8 D types) were used.

Figures 2 and 3 show the gray-level changes of a row of pixels of the MC involving ROIs of 2 mammograms belonging to the MIAS database. In the graphs, you can observe the sharply increasing peaks in the positions with MCs.

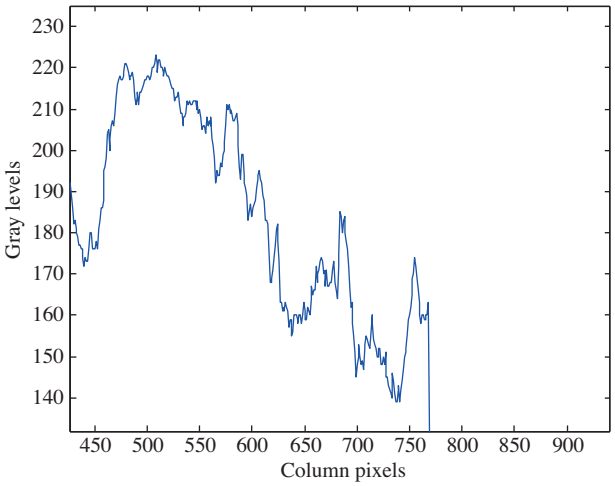

Figure 2. Row values of the mdb211 mammogram.

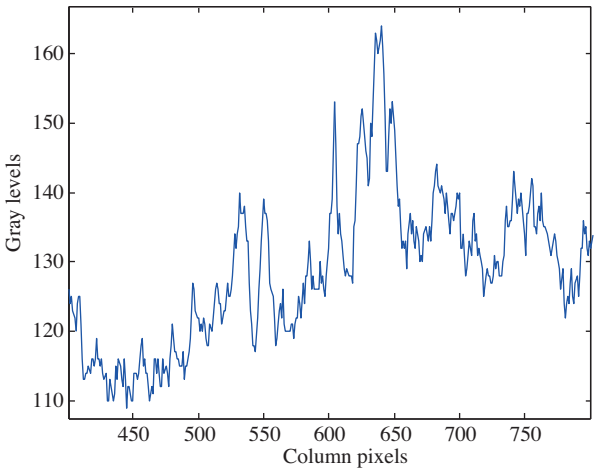

Figure 3. Row values of the mdb231 mammogram.

2.2. Methods

2.2.1. Preprocessing

Each pixel in an image means the probability of a 0.20-mm MC presence and any change in the gray level of the pixels will also negatively influence the region segmentation with MC. Therefore, no specific image processing algorithm has been applied to remove any imaging defect or noise.

Mammograms from the MIAS database involving malignant and benign MCs, and normal texture-type mammograms without MCs, are first put through a linear stretching process with values in the range of 0 to 255. Histogram stretching is performed to enhance the visibility of the MC structures in the digitized mammograms, providing greater separation between different gray levels by linearly remapping the pixel value from the minimum to maximum gray level, as given in Eq. (1).

In order to improve the recognition of the MC structures in the digitized mammograms, histogram stretching is applied. Thus, a significant difference between different gray levels is provided. The pixel values are linearly remapped from the minimum to maximum gray levels, as given in Eq. (1), using histogram stretching:

$$I_o(x,y) = 255.\frac{I_i(x,y) - \min}{\max - \min}, \tag{1}$$

where $I_o(x, y)$ is the gray level for the output pixel at (x, y) after the stretching process, $I_i(x, y)$ is the intensity value of a pixel at (x, y) in the digitized mammogram, and max and min are the highest and lowest gray-level values of the digitized mammogram, respectively.

After this process, the images whose MC locations are known ROIs of 50 $\times$ 50 pixels at different positions are chosen, where the clusters are not only at the center of the image but also at the side regions. As mentioned above, the selected tissue types and the distribution locations of the MC clusters are varied. A total of 57 ROIs are used, 33 with and 24 without MCs.

2.2.2. Contrast enhancement

In the first stage, to clarify the MC structures in the ROIs, the contrast is enhanced by unsharp masking, which is based on extracting the blurred state out of the image [35]. Unsharp masking is conducted using a Laplace filter. Since the Laplace operator given in Eq. (2) is a second-level derivative operation, it suppresses the slowly

changing gray levels while emphasizing the discontinuity of the gray levels. Since the gray-level change is high in the positions having MCs, these positions are seen as gray in the image that has gone through the Laplace filter. Normal texture regions are displayed in black because they involve less change. MC enhancement has been done by extracting the Laplace image from the original (ROI) image due to the negative filter coefficient at the center. Since the size of the smallest MC in the ROI is 1 pixel, a 3 $\times$ 3 pixel-sized Laplace filter is chosen. The alpha parameter in the Laplace filter controls the direction of the Laplacian (difference operation) and can be varied in the range of 0.0 to 1.0 for the unsharp masking. The 3 $\times$ 3 pixel-sized Laplace filter coefficients are: [–0.5 0 –0.5; 0, 3, 0; –0.5 0 –0.5]. The algorithm is run for the different values of the alpha and the results in Table 1 are obtained.

$$\nabla^2 = (\partial^2/\partial x^2) + (\partial^2/\partial y^2) \tag{2}$$

Figures 4 and 5 show the MC image in a mdb209 mammogram as its contrast is adjusted, which brings to the foreground the details of the same mammogram via unsharp masking.

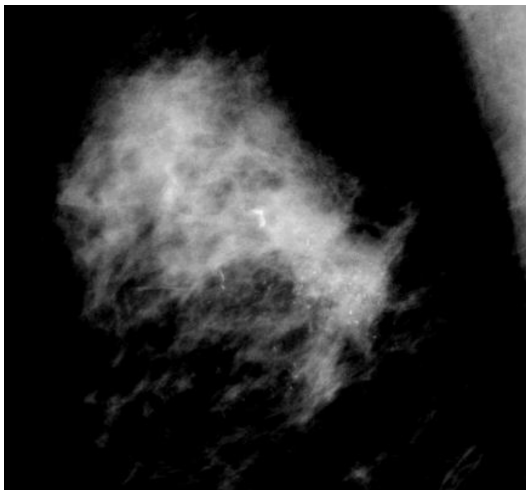

Figure 4. The mdb209 mammogram.

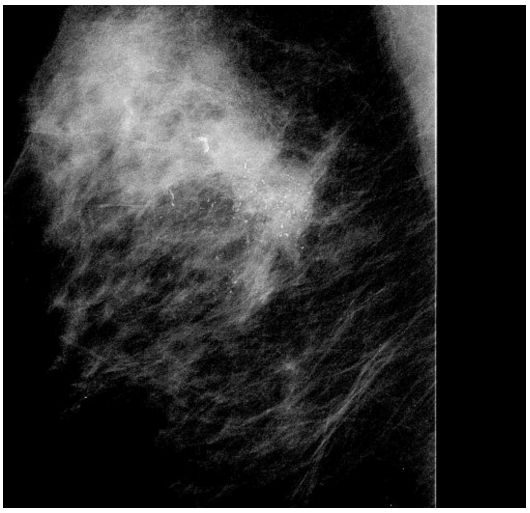

Figure 5. The mdb209 mammogram after unsharp masking.

Table 1. Mean TP variations at different alpha values.

alpha	Mean TP
0.1	0.9093
0.2	0.9254
0.3	0.9243
0.4	0.9225
0.5	0.9279
0.6	0.9289
0.7	0.9300
0.8	0.9361
0.9	0.9382
1	**0.9411**

2.2.3. Low-frequency elimination

The MCs in the ROIs whose contrast is adjusted appear at high spatial frequencies. In the second stage of this study, the images are decomposed into frequency components through multiresolution analysis. Low-frequency images of the ROIs are thought to explain the bulk breast tissue. The extraction of the normal tissue characteristics out of the ROI will make the MC structures more clarified and the statistical features more distinctive. Eltoukhy et al. [36] compared wavelet and curvelet transform for breast cancer diagnosis. Having defined the highest 100 coefficients as feature vectors, they determined that the successful classification rate of the curvelet transform coefficients is higher than that of the wavelet coefficients.

In this study, contourlet transform is used to determine the image having high spatial frequency regions. The contourlet transform, put forth by Do and Vetterli [37], was developed in the discrete domain via directional multiresolution filtering. There is an orthogonal version of the contourlet transform that is faster than the discrete curvelet algorithm. While the curvelet transform requires a circular operation in the 2-dimensional frequency domain at polar coordinates, the contourlet transform operates easily at rectangular coordinates. Therefore, it can be applied directly to digitized images.

Contourlet transform can extract the details in different directions, the edges that are not inclined in the same direction and the geometric features involving knowledge in the image. Although MCs have point-like appearances, they can be evaluated as objects having edges due to their forms with changing size. In wavelet transform, detailed horizontal, vertical, and diagonal images are decomposed in addition to the approximation image. As for the contourlet transform, the direction can be determined as far as the multiples of 2 for the straight angle. Thus, wavelets are usually successful at extracting point-like features, whereas contourlet transform is good at extracting line-like features in different directions.

In the proposed method, the ROI has undergone a filter bank process and has been decomposed into second-level subbands. In Figure 6, the image is decomposed into 2 pyramidal levels, 8 and 16 directional subbands. Since MCs are small in size and have a higher contrast compared to the tissues around them, they are expected to be viewed as high-frequency components. Therefore, the elimination of the low-frequency component in the contourlet transform will ensure the enhancement of the MCs.

In the filter bank, *db9.7* is used as the pyramid filter (Figure 7), since it has a linear phase, is close to orthogonal, and gives the best result [37]. For extracting information in different directions (Figure 8), the *pkva* ladder filter that was suggested by Phoong et al. [38] is used.

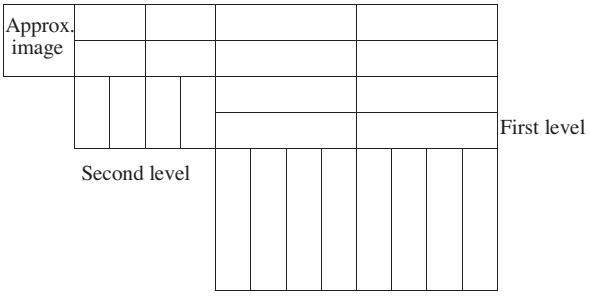

Figure 6. The 2-level contourlet transform.

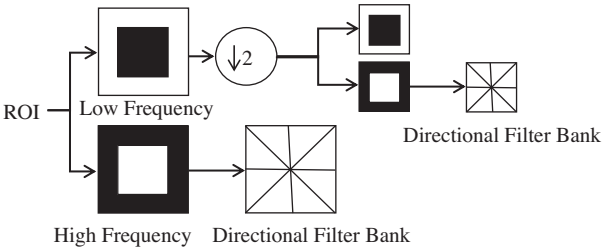

Figure 7. The 2-level contourlet transform subband decomposition.

In the subband image, while high-frequency coefficients are used without any change, the second-level approximation image is eliminated. The ROI is reconstructed from the coefficients whose low-frequency values are erased.

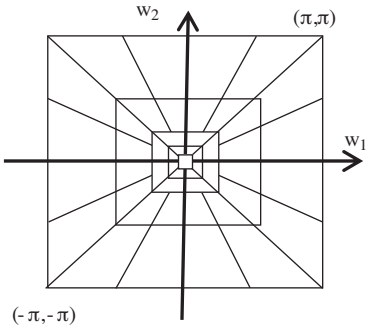

Figure 8. Directional filter frequency partition of the contourlet transform.

Shan et al. [39] compared wavelet, curvelet, and contourlet transform for denoising seismic waves. They stated that curvelet and contourlet transforms give better results than wavelets. In this study, both second-level contourlet transform and wavelet transform are applied using *db9.7* and *pkva* wavelets. In the first step, a ROI measuring 50 × 50 pixels is expanded to 64 × 64 pixels by copying the lateral pixels. Detailed images of the contourlet transform are obtained in 8 directions for the first (4 of them 8 × 16 pixels, and 4 of them 16 × 8 pixels in dimension) and 16 for the second level (8 of them 8 × 32 pixels, 8 of them 32 × 8 pixels in dimension). ROIs are reobtained by nullifying the coefficients of the 16 × 16 pixel-sized approximation images extracted at level 2.

2.2.4. Feature extraction

In ROIs with clarified structures of MCs, to seize the changes caused from the MCs, kurtosis, skewness, entropy, and energy criteria (Eqs. (3)–(6), respectively) of the distributions are investigated.

$$k = \frac{E(x-\mu)^4}{\sigma^4} \tag{3}$$

$$s = \frac{E(x-\mu)^3}{\sigma^3} \tag{4}$$

$$Ent = -\sum p \log_2(p) \tag{5}$$

$$E = \sum I(x,y)^2 \tag{6}$$

When the feature values are examined, first kurtosis and then skewness are observed as the most distinct statistics. As Gürcan et al. [11] stated, the statistical values of the regions without MCs seem to be closer to the statistical values of the Gaussian distribution, whereas those of the regions with MCs seem to differ.

2.2.5. Classification with support vector machines

To detect whether the ROIs whose statistical values are detected have MCs or not, and also to accurately classify the (background) regions without MCs, which cannot be defined by second-degree Gaussian statistics, normal distribution statistical values have not been taken as threshold values, because a support vector machine is used for classification, instead.

The reason why a support vector machine [40] is used for the classification of ROIs is its high performance in the literature. A support vector machine is based on structural risk minimization. It classifies by taking the

data to a higher dimensional space and forming a hyperplane [41,42]. While maximizing the distances of both classes to the hyperplane, it minimizes the distances of those belonging to the same class.

$$d(x) = \sum_{M}^{y_i} \alpha_i k(x, x_i) + b \tag{7}$$

In Eq. (7), k is the kernel function, b is the deviation value, and y is the class label. The sign of the function d(x) stands for the class membership of x. Where $\alpha_i \neq 0$, all x_i vectors show the support vectors of the most convenience. The performance of the method was compared when linear, polynomial, and quadratic functions are used as the kernel function of the support vector machine. The training and testing data to be used for this method were selected through a cross-validation technique. The training and testing data with a probability of 50% were picked out of a total of 57 ROIs, and after the support vector machine was trained with the data used as the training data, the classification was made on the remaining testing data.

2.3. Performance evaluation and comparison

The criteria used to report the performance of the algorithms related to the detection of cancer are the sensitivity and the number of FPs per image. A true positive (TP) rate is the number of signs detecting the presence of cancer accurately. Sensitivity is the rate of detecting the TPs from all of the data with cancer (Eq. (9)), and this is defined as the TP rate. A FP is the warning of cancer despite there being no cancer. The FP value is at the same time calculated via the formula 1 – specificity (Eq. (10)).

$$sensitivity = \frac{TP}{TP + FN} \tag{8}$$

$$FP = 1 - specificity = 1 - \frac{TN}{TN + FP} = \frac{FP}{TN + FP} \tag{9}$$

This study has taken the TP rate and FP amount per image as a basis in the classification of ROIs depending on the presence of MCs in order to be able to compare with the other methods.

3. Results

In the first stage, the influence of the process of sharpening on the TP rate is examined. When MC detection in ROIs is done without the sharpening process, the TP rate is 91% and the FP value is 0.09 as a result of 100 iterative classifications. When the sharpening step is added, the TP rate is 94% and the FP becomes 0.06. The sharpening process thus increases the achievement rate in the detection of MCs. The mean classification confusion matrix for the second situation is given in Table 2.

Table 2. Mean classification confusion matrix.

		Ground truth	
		With MC	Without MC
Classification result	With MC	11.22 (TP)	0.97 (FP)
	Without MC	0.78 (FN)	15.03 (TN)

In this study, both the second-level contourlet transform and the wavelet transform reveal the same performance for the MC detection in this database and the selected size of the ROIs. To achieve a more general solution for the MC detection and cover other types of databases, the contourlet transform is used.

At the second stage, the influence on TP rate of the selection of kernel functions used in the support vector machine for the classification is investigated in MATLAB. The TP rate graph obtained as a result of 100 iterative classifications made by the support vector machine using linear kernel function is given in Figure 9. The average TP is 94%.

The TP rate graph obtained after 100 iterative classifications made by the support vector machine using a polynomial kernel function is given in Figure 10. The average TP is 93%.

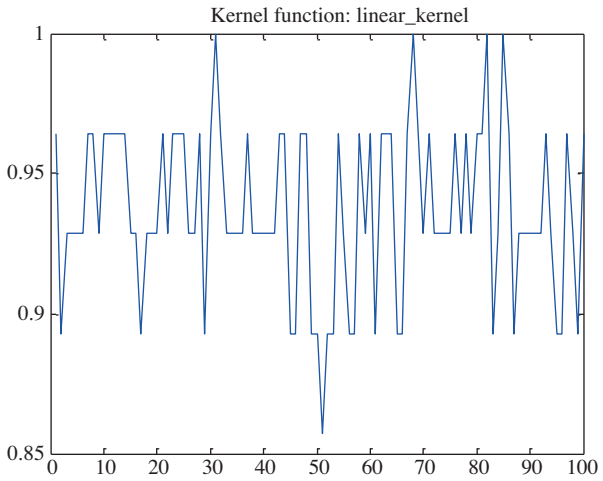

Figure 9. TP rate for the support vector machine using the linear kernel function.

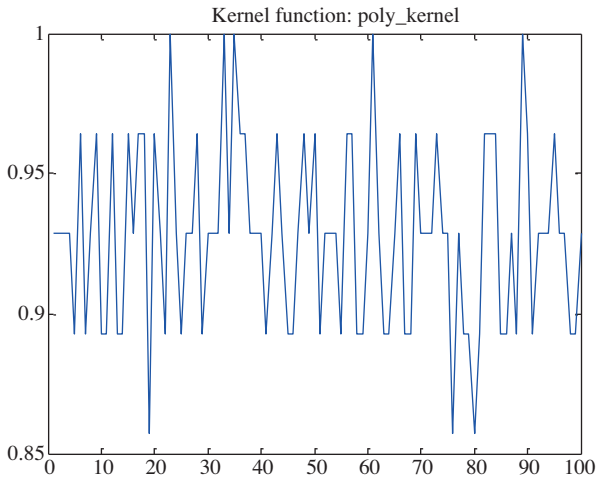

Figure 10. TP rate with the polynomial kernel function support vector machine.

The resulting average TP rate of 100 iterative classifications made by the support vector machine using a quadratic kernel function is 91%. There are decreasing values in the TP rates, reaching down as far as 75%. The classification made by the support vector machine using a linear kernel turns out to have a slightly higher TP rate than the others.

Figures 11 and 12 show the values, measured only once, of the features extracted from the image reconstructed in the contourlet transform after the approximation coefficients are eliminated. Of the 57 ROIs,

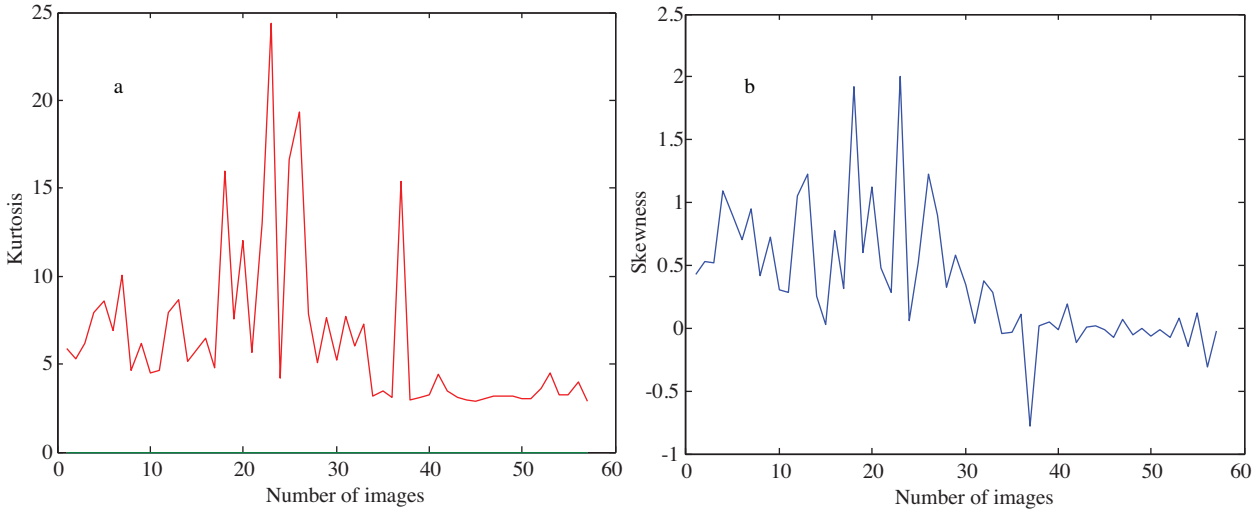

Figure 11. Kurtosis (a) and skewness (b).

1–21 are malignant, 22–33 are benign, and 34–57 are normal. When the graphs of the kurtosis and skewness features are studied, it is seen that there is a discernible difference between the ROIs with and without MCs. Since there are sharpening and subband erasing processes that strengthen the data irregularities in the algorithm, entropy seems to make no distinction between the ROIs with and without MCs. As for the energy values, although not as much so as in the features of kurtosis and skewness, there is a discernible difference in the graph.

This study gives, in Table 3, a comparison of the method suggested for MC detection and other methods put forward in recent years to be used by computer-aided systems.

Table 3. Comparison of the MC detection methods.

Study	Method	Database, number of ROIs	TP (%)	FP	Year
The proposed method	Unsharp masking, low-band elimination using contourlet transform, feature extraction, ROI classification using support vector machine.	MIAS, 57	94	0.06	2012
Yu and Guan [3]	Wavelet transform, segmentation using statistical features, 31 feature extractions, feature selection using neural network.	Nijmegen, 40	90	0.5	2000
Jing et al. [4]	Gray-level distribution modeling (MCs are modeled with gamma, background is modeled by Gaussian), the spatial distribution and amplitude parameter extraction of the clustered MCs, maximum a posteriori estimation.	141	90	0.5	2011
Halkiotis et al. [5]	Mathematical morphology, artificial neural network.	-	94.7	0.27	2007
Yu and Huang [6]	Wavelet filter and thresholding, model-based and statistical texture features.	MIAS, 20	94 90	1 0.65	2010
Sankar and Thomas [15]	Fractal analysis.	-	91.81	-	2010
Oliver et al. [17]	Local feature extraction via filtering.	3 databases, 2 of them digitized afterwards	80	1	2012
Rizzi et al. [22]	Biorthogonal and orthogonal wavelet filter, thresholding.	-	98 95	1 0.5	2009
Peng et al. [24]	Knowledge-discovery mechanism in the genetic algorithm.	DDSM	96.8 98.9	0.20 0.4	2006
Mohanalin et al. [32]	Tsallis entropy, type II fuzzy index for thresholding.	UCSF and MIAS, 247	96.55	0.4	2010
Dheeba and Tamil [33]	Feature extraction using Law's texture energy measures, pixel classification via support vector machine.	MIAS	86.1	-	2011

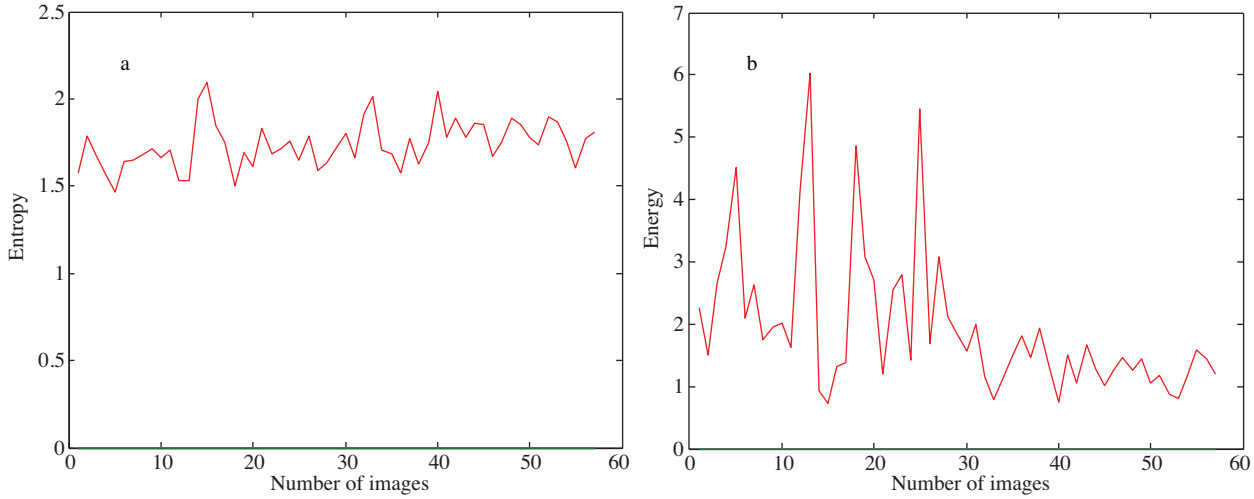

Figure 12. Entropy (a) and energy (b).

4. Conclusion

In this study, for fully automated MC cluster detection, unsharp masked and low-band eliminated images' extracted features were classified using support vector machines on the MIAS database, consisting of normal mammograms together with benign and malignant mammograms involving MCs. The ROIs, sharpened using a Laplace filter-based unsharp masking method, were put through a subband decomposition process and then, by eliminating the approximation image, the features were detected from the reconstructed image. For classifying the testing data, a support vector machine, trained by the data picked among 57 ROIs through a cross-validation method, was used.

Due to the difficulty of detecting MCs rendered by the density of the texture, the focus was especially placed on the samples containing dense textures. The D-type texture ratio was 24/57. In ROI selection, to ensure the independence of each datum from each other, one ROI out of each MC cluster was picked. In the case of the MCs distributed in a large area in the mammograms, more than one ROI was picked from the same mammogram, provided that they were in positions that did not overlap.

In the method proposed, first, the MC structures were further clarified, and then the texture that they form with the texture surrounding these structures was analyzed. For classification, a feature-based approach was used: while the gray levels in the normal texture showed smooth rises and falls, the statistical features were observed to be close to a Gaussian distribution, but in the regions of irregularities involving regional maximums like MCs, they diverged from the Gaussian distribution. In this method, the inadequacy of the non-MC noisy background regions (described by second-order Gaussian statistics) is compensated for by the generalization ability of the support vector machines.

The method proposed does not, at any stage, involve any presupposed value of a parameter or a situation dependent on the database. The ROI dimension and filter size are determined according to the database pixel resolution, based on the MC dimension and MC cluster definition.

In conclusion, in this method, no user interaction is required and all of the steps are implemented automatically. Selecting the threshold or obtaining image-dependent parameters is not necessary in the presented method. Moreover, this method is much easier to implement compared to the others. Thus, it is appropriate for real-time clinical applications. Future studies will focus on testing the method in different databases and increasing the MC detection rate.

Acknowledgment

The authors acknowledge the retrieval of the MIAS database from the Internet for the experiments described in this paper and wish to thank the NCR MRI Diagnosis Center, NIT, Faridabad, India, for permitting us to use their databases.

References

[1] American Cancer Society, Cancer Facts and Figures 2011, Atlanta, GA, USA, ACS, 2011. Available at http://www.cancer.org/acs/groups/content/@epidemiologysurveilance/documents/document/acspc-029771.pdf.

[2] D.B. Kopans, Breast Imaging, Philadelphia, PA, USA, Lippincott Williams & Wilkins, 1998.

[3] S. Yu, L. Guan, "A CAD system for the automatic detection of clustered microcalcifications in digitized mammogram films", IEEE Transactions on Medical Imaging, Vol. 19, pp. 115–126, 2000.

[4] H. Jing, Y. Yang, R.M. Nishikawa, "Detection of clustered microcalcifications using spatial point process modeling", Physics in Medicine and Biology, Vol. 56, pp. 1–17, 2011.

[5] S. Halkiotis, T. Botsis, M. Rangoussi, "Automatic detection of clustered microcalcifications in digital mammograms using mathematical morphology and neural networks", Signal Processing, Vol. 87, pp. 1559–1568, 2007.

[6] S.N. Yu, Y.K. Huang, "Detection of microcalcifications in digital mammograms using combined model-based and statistical textural features", Expert Systems with Applications, Vol. 37, pp. 5461–5469, 2010.

[7] R.M. Nishikawa, M.L. Giger, K. Doi, C.J. Vyborny, R.A. Schmidt, "Computer-aided detection of clustered microcalcifications on digital mammograms", Medical & Biological Engineering & Computing, Vol. 33, pp. 174–178, 1995.

[8] K.J. McLoughlin, P.J. Bones, N. Karssemeijer, "Noise equalization for detection of microcalcification clusters in direct digital mammogram images", IEEE Transactions on Medical Imaging, Vol. 23, pp. 313–320, 2004.

[9] W. Qian, F. Mao, X. Sun, Y. Zhang, D. Song, R.A. Clarke, "An improved method of region grouping for microcalcification detection in digital mammograms", Computerized Medical Imaging and Graphics, Vol. 26, pp. 361–368, 2002.

[10] M.G. Linguraru, K. Marias, R. English, M. Brady, "A biologically inspired algorithm for microcalcification cluster detection", Medical Image Analysis, Vol. 10, pp. 850–862, 2006.

[11] M.N. Gürcan, Y. Yardımcı, A.E. Çetin, R. Ansari, "Detection of microcalcifications in mammograms using higher order statistics", IEEE Signal Processing Letters, Vol. 4, pp. 213–216, 1997.

[12] M.N. Gürcan, Y. Yardımcı, A.E. Çetin, R. Ansari, "Automated detection and enhancement of microcalcifications in mammograms using nonlinear subband decomposition", IEEE International Conference on Acoustics, Speech, and Signal Processing, Vol. 4, pp. 3069–3072, 1997.

[13] B. Caputo, E.L. Torre, S. Bouattour, G.E. Gigante, "A new kernel method for microcalcification detection: Spin glass-Markov random fields," Studies in Health Technology and Informatics, Vol. 90, pp. 30–34, 2002.

[14] P. Casaseca-de-la-Higuera, J.I. Arribas, E. Munoz-Moreno, C. Alberola-Lopez, "A comparative study on microcalcification detection methods with posterior probability estimation based on Gaussian mixture models", Proceedings of the Annual International Conference of the IEEE Engineering in Medicine and Biology Society, Vol. 1, pp. 49–54, 2005.

[15] D. Sankar, T. Thomas, "A new fast fractal modeling approach for the detection of microcalcifications in mammograms", Journal of Digital Imaging, Vol. 23, pp. 538–546, 2010.

[16] J. Huang, J. Li, T. Liu, "A new fast fractal coding method for the detection of microcalcifications in mammograms", International Conference on Multimedia Technology, pp. 4768–4771, 2011.

[17] A. Oliver, A. Torrent, X. Lladó, M. Tortajada, L. Tortajada, M. Sentís, J. Freixenet, R. Zwiggelaar, "Automatic microcalcification and cluster detection for digital and digitised mammograms", Knowledge-Based Systems, Vol. 28, pp. 68–75, 2012.

[18] R.N. Strickland, H. Hahn, "Wavelet transforms for detecting microcalcifications in mammograms", IEEE Transactions on Medical Imaging, Vol. 15, pp. 218–229, 1996.

[19] M.G. Mini, V.P. Devassia, T. Thomas, "Multiplexed wavelet transform technique for detection of microcalcification in digitized mammograms", Journal of Digital Imaging, Vol. 17, pp. 285–291, 2004.

[20] R. Nakayama, Y. Uchiyama, K. Yamamoto, R. Watanabe, K. Namba, "Computer-aided diagnosis scheme using a filter bank for detection of microcalcification clusters in mammograms", IEEE Transactions on Biomedical Engineering, Vol. 53, pp. 273–283, 2006.

[21] E. Regentova, L. Zhang, J. Zheng, G. Veni, "Microcalcification detection based on wavelet domain hidden Markov tree model: study for inclusion to computer aided diagnostic prompting system", Medical Physics, Vol. 34, pp. 2206–2219, 2007.

[22] M. Rizzi, M. D'Aloia, B. Castagnolo, "Computer aided detection of microcalcifications in digital mammograms adopting a wavelet decomposition", Integrated Computer-Aided Engineering, Vol. 16, pp. 91–103, 2009.

[23] J. Jiang, B. Yao, A.M. Wason, "A genetic algorithm design for microcalcification detection and classification in digital mammograms", Computerized Medical Imaging and Graphics, Vol. 31, pp. 49–61, 2007.

[24] Y. Peng, B. Yao, J. Jiang, "Knowledge-discovery incorporated evolutionary search for microcalcification detection in breast cancer diagnosis", Artificial Intelligence in Medicine, Vol. 37, pp. 43–53, 2006.

[25] L. Bocchi, G. Coppini, J. Nori, G. Vali, "Detection of single and clustered microcalcifications in mammograms using fractals models and neural networks", Medical Engineering & Physics, Vol. 26, pp. 303–312, 2004.

[26] M.N. Gürcan, H.P. Chan, B. Sahiner, L. Hadjiiski, N. Petrick, M.A. Helvie, "Optimal neural network architecture selection: Improvement in computerized detection of microcalcifications", Academic Radiology, Vol. 9, pp. 420–429, 2002.

[27] A. Papadopoulos, D.I. Fotiadis, A. Likas, "An automatic microcalcification detection system based on a hybrid neural network classifier", Artificial Intelligence In Medicine, Vol. 25, pp. 149–167, 2002.

[28] P. Sajda, C. Spence, J. Pearson, "Learning contextual relationships in mammograms using a hierarchical pyramid neural network", IEEE Transactions on Medical Imaging, Vol. 21, pp. 239–250, 2002.

[29] I. El Naqa, Y. Yang, M.N. Wernick, N.P. Galatsanos, R.M. Nishikawa, "A support vector machine approach for detection of microcalcifications", IEEE Transactions on Medical Imaging, Vol. 21, pp. 1552–1563, 2002.

[30] L. Wei, Y. Yang, R. M. Nishikawa, M.N. Wernick, A. Edwards, "Relevance vector machine for automatic detection of clustered microcalcifications", IEEE Transactions on Medical Imaging, Vol. 24, pp. 1278–1285, 2005.

[31] I.I. Andreadis, G.M. Spyrou, K.S. Nikita, "A comparative study of image features for classification of breast microcalcifications", Measurement Science and Technology, Vol. 22, pp. 114005–114014, 2011.

[32] B. Mohanalin, P.K. Karla, N. Kumar, "A novel automatic microcalcification detection technique using Tsallis entropy & a type II fuzzy index", Computers and Mathematics with Applications, Vol. 60, pp. 2426–2432, 2010.

[33] J. Dheeba, S.S. Tamil, "Classification of malignant and benign microcalcification using SVM classifier", Emerging Trends in Electrical and Computer Technology, 2011.

[34] J. Suckling, J. Parker, D.R. Dance, S. Astley, I. Hutt, "The mammographic image analysis society digital mammogram database", 2nd International Workshop on Digital Mammography, pp. 375–378, 1994.

[35] R.C. Gonzalez, R.E. Woods, Digital Image Processing, 2nd ed., Upper Saddle River, NJ, USA, Prentice Hall, 2002.

[36] M.M. Eltoukhy, I. Faye, B.B. Samir, "A comparison of wavelet and curvelet for breast cancer diagnosis in digital mammogram", Computers in Biology and Medicine, Vol. 40, pp. 384–391, 2010.

[37] M. Do, M. Vetterli, "The contourlet transform: an efficient directional multiresolution image representation", IEEE Transactions on Image Processing, Vol. 14, pp. 2091–2106, 2005.

[38] S.M. Phoong, C.W. Kim, P.P. Vaidyanathan, R. Ansari, "A new class of two channel biorthogonal filter banks and wavelet basis", IEEE Transactions on Signal Processing, Vol. 43, pp. 649–665, 1995.

[39] H. Shan, J. Ma, H. Yang, "Comparisons of wavelets, contourlets and curvelets in seismic denoising", Journal of Applied Geophysics, Vol. 69, pp. 103–115, 2009.

[40] V.N. Vapnik, "An overview of statistical learning theory", IEEE Transactions on Neural Networks, Vol. 10, pp. 988–999, 1999.

[41] T. Joachims, "Making large-scale support vector machine learning practical", in: B. Schölkopf, C. Burges, A. Smola, editors, Advances in Kernel Methods - Support Vector Learning, Cambridge, MA, USA, MIT Press, pp. 169–184, 1999.

[42] N. Acır, "Classification of ECG beats by using a fast least square support vector machines with a dynamic programming feature selection algorithm", Neural Computing & Applications, Vol. 14, pp. 299–309, 2005.